PAPER

Characterization of the liquid Li-solid Mo (1 1 0) interface from classical molecular dynamics for plasma-facing applications

To cite this article: Joseph R. Vella *et al* 2017 *Nucl. Fusion* **57** 116036

View the article online for updates and enhancements.

Characterization of the liquid Li-solid Mo (1 1 0) interface from classical molecular dynamics for plasma-facing applications

Joseph R. Vella[1], **Mohan Chen**[2,a], **Sven Fürstenberg**[1],
Frank H. Stillinger[3], **Emily A. Carter**[4], **Pablo G. Debenedetti**[1]
and Athanassios Z. Panagiotopoulos[1,b]

[1] Department of Chemical and Biological Engineering, Princeton University, Princeton, New Jersey 08544, United States of America
[2] Department of Mechanical and Aerospace Engineering, Princeton University, Princeton, New Jersey 08544, United States of America
[3] Department of Chemistry, Princeton University, Princeton, New Jersey 08544, United States of America
[4] School of Engineering and Applied Science, Princeton University, Princeton, New Jersey 08544, United States of America

E-mail: azp@princeton.edu

Abstract

An understanding of the wetting properties and a characterization of the interface between liquid lithium (Li) and solid molybdenum (Mo) are relevant to assessing the efficacy of Li as a plasma-facing component in fusion reactors. In this work, a new second-nearest neighbor modified embedded-atom method (2NN MEAM) force field is parameterized to describe the interactions between Li and Mo. The new force field reproduces several benchmark properties obtained from first-principles quantum mechanics simulations, including binding curves for Li at three different adsorption sites and the corresponding forces on Li atoms adsorbed on the Mo (1 1 0) surface. This force field is then used to study the wetting of liquid Li on the (1 1 0) surface of Mo and to examine the Li–Mo interface using molecular dynamics simulations. From droplet simulations, we find that liquid Li tends to completely wet the perfect Mo (1 1 0) surface, in contradiction with previous experimental measurements that found non-zero contact angles for liquid Li on a Mo substrate. However, these experiments were not carried out under ultra-high vacuum conditions or with a perfect (1 1 0) Mo surface, suggesting that the presence of impurities, such as oxygen, and surface structure play a crucial role in this wetting process. From thin-film simulations, it is observed that the first layer of Li on the Mo (1 1 0) surface has many solid-like properties such as a low mobility and a larger degree of ordering when compared to layers further away from the surface, even at temperatures well above the bulk melting temperature of Li. These findings are consistent with temperature-programmed desorption experiments.

S Supplementary material for this article is available online

(Some figures may appear in colour only in the online journal)

---

[a] Current address: Department of Physics, Temple University, Philadelphia, PA 19122, United States of America
[b] Author to whom any correspondence should be addressed.

1. Introduction

Molybdenum (Mo) and other refractory metals (such as tungsten) have received a lot of attention for their use in the inner walls and divertors of tokamak reactors [1–5]. However, solid materials face many hurdles when exposed to reactor operation conditions. For example, it is known that tungsten becomes brittle when exposed to neutrons ejected from the plasma [6]. Deuterium and tritium ions will also pose a problem as they will weaken the mechanical properties of solid metals and are challenging to remove [7, 8]. Due to these challenges, attention has shifted to using liquid metals as plasma-facing materials [6, 9, 10].

Lithium (Li) is one of the most promising liquid metal plasma-facing components due to several favorable properties such as its relatively low melting temperature (compared to other metals) and its reactivity towards hydrogen and its isotopes. The high reactivity of Li allows the tokamak reactor to operate in the 'low recycle' regime, meaning particles expelled from the plasma rarely return [11, 12]. However, further investigation is needed of various phenomena in order to fully understand the potential use of Li as a plasma-facing component. One such example is the wetting behavior of Li on relevant solid substrates and characterization of the solid-liquid interface.

Experimental work by Fiflis *et al* [13] examined the contact angle of liquid Li on a variety of solid surfaces relevant to fusion reactors including Mo. However, these experiments lack the atomistic detail that simulation studies can provide. Recently, a joint experimental/simulation study examined the interaction between Li atoms and the Mo (1 1 0) surface using temperature-programmed desorption and Kohn–Sham density functional theory (KSDFT) [14]. First-principles quantum mechanics simulation methods, such as KSDFT, are computationally expensive and thus there are limits on the system size and timescale able to be simulated. Classical mechanics methods are less computationally expensive when compared to quantum mechanics techniques and can simulate larger system sizes and access longer timescales. However, these methods require the specification of a force field in order to quantify the interactions between atoms. These force fields typically require experimental data or quantum mechanics calculations to fit several parameters.

In this work, we present a classical force field describing the interaction between Li and Mo atoms, which was fit to KSDFT data. The force fields for Li–Li interactions and Mo–Mo interactions are taken from previous work, as explained in the next section. The type of force fields utilized are second-nearest neighbor modified embedded-atom method (2NN MEAM) potentials. These force fields are used to study the wetting behavior of liquid Li on the Mo (1 1 0) surface and to characterize the interface using molecular dynamics (MD).

The paper is organized as follows. The 'Force field development' section briefly describes the 2NN MEAM formalism, the KSDFT calculations, and the optimization procedure used to fit parameters for the Li–Mo interaction. The 'Classical simulations' section describes details of classical MD simulations used to study the wetting behavior and characteristics of

Table 1. 2NN MEAM parameters for the force fields used in this work. Note r_e corresponds to the nearest-neighbor distance of the reference lattice structure. bcc and b2 refer to body-centered cubic and CsCl lattice structures, respectively. The functional forms of each of the terms in the 2NN MEAM force field is given by Lee and Baskes [15].

Pure elements	Li	Mo	Cross terms	Li/Mo
α	3.00	5.84	α	4.38
E_c	1.65	6.81	E_c	3.84
r_e	2.99	2.73	r_e	2.89
r_c	4.8	4.8	r_c	4.8
d	0.139	0.00	d	0.07
Δr	0.2	0.2	Δr	0.2
Reference lattice	bcc	bcc	Reference lattice	b2
A	0.64	0.46	ρ_{Mo}/ρ_{Li}	1.309
$\beta^{(0)}$	1.03	7.03	$C_{min}(1,1,2)$	1.12
$\beta^{(1)}$	4.88	1.00	$C_{max}(1,1,2)$	2.80
$\beta^{(2)}$	4.15	1.00	$C_{min}(2,2,1)$	0.05
$\beta^{(3)}$	5.27	1.00	$C_{max}(2,2,1)$	2.05
$t^{(0)}$	1.00	1.00	$C_{min}(1,2,1)$	1.71
$t^{(1)}$	−1.46	0.50	$C_{max}(1,2,1)$	2.54
$t^{(2)}$	4.13	3.10	$C_{min}(1,2,2)$	0.31
$t^{(3)}$	−0.57	−7.50	$C_{max}(1,2,2)$	2.80
C_{max}	1.91	2.80	—	—
C_{min}	0.31	0.64	—	—

the Li–Mo interface. That section also presents results from these simulations. The 'Concluding remarks' section summarizes and interprets the findings, and provides suggestions for future work.

2. Force field development

2.1. Force field

In this work, 2NN MEAM force fields were used to describe all interactions for classical simulations. The potential energy using the 2NN MEAM force fields is given by

$$E_{pot} = \sum_j G_j(\phi_j) + \frac{1}{2} \sum_j \sum_{k \neq j} \varphi_{jk}(r_{jk}). \quad (1)$$

G_j is the embedding energy of atom j and is seen as the energy it takes to embed atom j into a effective background electron density ϕ_j imposed by surrounding atoms. The embedding energy typically accounts for metallic bonding. $\varphi_{jk}(r_{jk})$ is a pairwise potential which can be interpreted as the effective electrostatic interactions between the cores of atoms j and k which are separated by a distance r_{jk}.

There are several parameters that govern the behavior of the embedding energy, effective background electron density, and pairwise potential. These parameters are chosen such that the 2NN MEAM force fields give good agreement with experimental or quantum mechanical data. The functional forms of each of the terms can be found in the original 2NN MEAM paper [15]. The parameters for all interactions are given in table 1. The force fields were implemented in LAMMPS

[16] (15 May 2015 version). The LAMMPS force field files are available as supplementary materials (stacks.iop.org/NF/57/116036/mmedia).

For Li–Li interactions we employed the potential developed by Cui *et al* [17], while for Mo–Mo interactions the potential developed by Lee *et al* [18] was used. Two parameters of the Mo–Mo force field, r_c and Δr, were changed to match those assigned to the Li–Li force field. This was done because LAMMPS [16] assigns a global value of r_c and Δr to all atom types. Changing the values of these parameters did not significantly affect any of properties reported in the original Mo work. The parameters for the Li–Mo interactions were developed in this work. The quantum mechanics calculations used to fit the Li–Mo interactions, benchmarking results, and optimization procedure are described in the next section.

2.2. Quantum mechanics calculations and optimization

This section briefly discusses the quantum mechanics calculations used for fitting the parameters for Li–Mo interactions. For more details, we refer to the reference by Chen *et al* [14] where a similar procedure and setup was adopted. All calculations were performed using KSDFT. These calculations were carried out using the Vienna *ab initio* simulation package (VASP, version 5.3.5) [19–21]. The plane-wave basis set had a kinetic energy cutoff of 400 eV. This energy cutoff converges the total energies of both bcc Mo and bcc Li to within 1 meV atom^{-1}. The Perdew–Burke–Ernzerhof (PBE) [22] form of the generalized-gradient approximation exchange-correlation functional was employed and default projector-augmented-wave (PAW) [23] potentials with atomic configurations [Mo]4d^{5}5s^1 and [Li]2s^1 were used to represent the valence-electron—screened-ion (core electrons plus nucleus) interactions. We chose the Monkhorst–Pack scheme [24] and Methfessel–Paxton smearing method [25] (with a smearing width of 0.05 eV) for sampling k-point meshes in the Brillouin zone and integration of the Brillouin zone, respectively.

Parameters for Li–Mo interactions were optimized to reproduce KSDFT-PBE adsorption energies for Li atoms adsorbed on the Mo (1 1 0) surface at various sites and coverages, as well as forces experienced by the atoms. KSDFT-PBE is a credible benchmark theory, as it has been demonstrated to accurately predict structural properties of Li on Mo and has also been used to explain temperature-dependent Li desorption behavior on the Mo (1 1 0) surface [14].

For the KSDFT calculations, a seven-layer slab of Mo atoms, with the bottom three layers held fixed, was set up on a bcc lattice in a periodic box such that the [1 1 0] direction was oriented in the *z* direction. A vacuum region extending 10 Å in the *z* direction was present above the exposed surface. The vacuum region was large enough such that the slab did not interact with its periodic images in the *z* direction. This was verified by performing identical simulations with a larger vacuum region thickness (15 Å). These simulations produced results identical to those with the vacuum region extending 10 Å. Li atoms were then placed on one of three adsorption sites at various coverages. The adsorption sites considered were
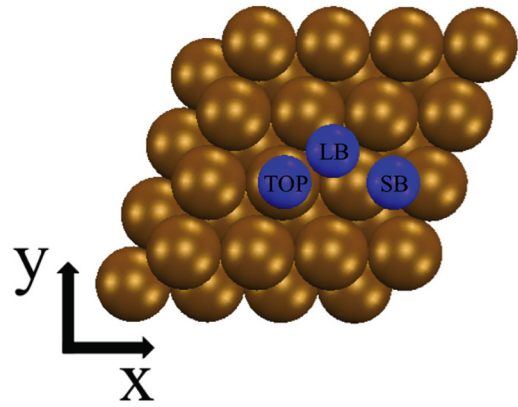
Figure 1. A snapshot showing the long-bridge (LB), short-bridge (SB), and top (TOP) adsorption sites on the (1 1 0) Mo surface. Blue spheres are Li atoms and brown spheres are Mo atoms. Snapshots were rendered in visual molecular dynamics (VMD) [26].

long-bridge (LB), short-bridge (SB), and top (TOP) sites. The adsorption sites are shown in figure 1.

For each of these adsorption sites, three coverages were considered, $\theta = 1.00, 0.50,$ and 0.25, where $\theta = 1.00$ corresponds to a monolayer. The k-point mesh was set to $18 \times 18 \times 1$ for a coverage of 1.00 and $9 \times 9 \times 1$ for coverages 0.50 and 0.25. The choice of k-point meshes for coverages 1.00 and 0.25 were taken from the work of Chen *et al* [14]. The coverage of 0.50 used the same choice of k-point mesh used by the coverage of 0.25 because the cells are the same (except the cell with a coverage of 0.50 contains one extra Li atom). The k-point meshes were chosen such that the total energies of the systems are converged to within 1 meV atom^{-1}. For $\theta = 1.00$, simulations contained 7 Mo atoms and 1 Li atom, for $\theta = 0.50$, simulations contained 28 Mo atoms and 2 Li atoms, and for $\theta = 0.25$, simulations contained 28 Mo atoms and 1 Li atom. Coverages lower than 0.25 were not considered because we are mainly interested in the wetting of liquid Li and properties of a Li thin film on the Mo (1 1 0) surface, i.e., high coverages. For the SB and TOP sites, at each coverage, five distances between the Mo slab and Li layer were considered during the optimization procedure: 2.0, 2.5, 3.0, 3.5, and 4.5 Å. Since the LB site was found to be the most stable adsorption site for Li on the Mo (1 1 0) surface in the coverage range from 1.0 to 0.06 [14], we also chose one geometry with the Li layer located at the LB site at 2.2 Å above the surface. This distance is closer to the equilibrium distance for a wide range of coverages, which varies from 2.229 to 2.376 Å when Li coverage changes from 1.0 to 0.06 as obtained from KSDFT [14]. For $\theta = 1.00$ and $\theta = 0.25$, one Li atom is placed on (1×1) or (2×2) Mo (1 1 0) surface unit cells, respectively. The geometry with $\theta = 0.50$ was generated by placing two Li atoms with a distance of $\sqrt{2}a$ (*a* being the lattice constant of bcc Mo) between them on a (2×2) Mo (1 1 0) surface unit cell. Thus, a total of 48 geometries were used in the training set for the parameterization of the Li–Mo force field. The adsorption energy and forces on Li atoms were computed for each of the 48 geometries and served as target values during fitting of force-field parameters. The adsorption energy is defined as

$$E_{\text{ads}} = E_{\text{Li/Mo}(1\,1\,0)} - E_{\text{Mo}(1\,1\,0)} - E_{\text{Li}}, \qquad (2)$$

where E_{ads} is the adsorption energy of a certain coverage of Li, $E_{\text{Li/Mo}(1\,1\,0)}$ is the energy of a Mo (1 1 0) slab with adsorbed Li, $E_{\text{Mo}(1\,1\,0)}$ is the energy of an isolated Mo slab, and E_{Li} is the energy of an isolated Li atom. The forces acting on the Li atoms can be directly extracted from KSDFT calculations.

The optimization was performed using a simulated annealing procedure [27]. The target function that is minimized has the form of

$$\prod(\mathbf{x}) = \sum_{i=1}^{N} w_i |y_i - f_i(\mathbf{x})|, \qquad (3)$$

where N is the total number of properties and w_i is a weighting factor for property i. y_i is a target value (either adsorption energy or forces on Li atoms) from KSDFT calculations, and $f_i(\mathbf{x})$ is the same property obtained from 2NN MEAM calculations using a parameter set $\mathbf{x}$. $w_i = 1.0$ is used for both adsorption energies and forces on Li atoms for SB and TOP sites, and $w_i = 6.0$ is used for these properties for the LB site. During the optimization procedure, the weight on the properties for the LB site was increased until the new force field sufficiently reproduced the adsorption energy curves for the LB site because it is the most stable adsorption site. The main purpose of including the adsorption energy curves for the SB and TOP sites in our optimization was to ensure the energy ordering between the three adsorption sites was captured.

Figure 2 shows the adsorption energy curves from KSDFT calculations and the new Li–Mo 2NN MEAM force field for various adsorption sites and coverages. Although the new Li–Mo force field does not quantitatively reproduce the adsorption energy curves, it does qualitatively capture some important features. For example, the energy orderings of LB, SB, and TOP sites are reproduced, where the LB site is the most stable adsorption site. The equilibrium Li–Mo distances are also accurately captured, with the largest discrepancies occurring for low coverages. Note that for $\theta = 0.25$, there are discontinuities in the adsorption energy curves that appear beyond 3 Å. The origin of these discontinuities appears to originate from the Li force field by Cui *et al* [17]. The adsorption energy curves at $\theta = 0.25$ were recalculated for Li adsorbed on a Li slab, Mo adsorbed on a Mo slab, and Mo adsorbed on a Li slab. Similar discontinuities are only observed for the curves corresponding to Li adsorbed on a Li slab. It seems the Cui Li force field is not suited for modeling Li atoms adsorbed on surfaces at low coverages, leading to the discontinuities seen in figure 2. However, the parameters of the Li–Li interactions were not changed in the optimization procedure, so we did not explore if the discontinuities could be eliminated. We point out that this should have no significant effects in our study of wetting properties of Li, because the coverage stays high once Li wets Mo surfaces. This will be shown in the next section.

Table 2 provides the numerical results for the adsorption energies and the minimum energy Li–Mo distances for different adsorption sites on the Mo (1 1 0) surface taken from figure 2. The differences between the adsorption energy for KSDFT and 2NN MEAM for $\theta = 1.0$ and 0.50 at the LB site are both smaller than 0.06 eV, and the corresponding Li–Mo
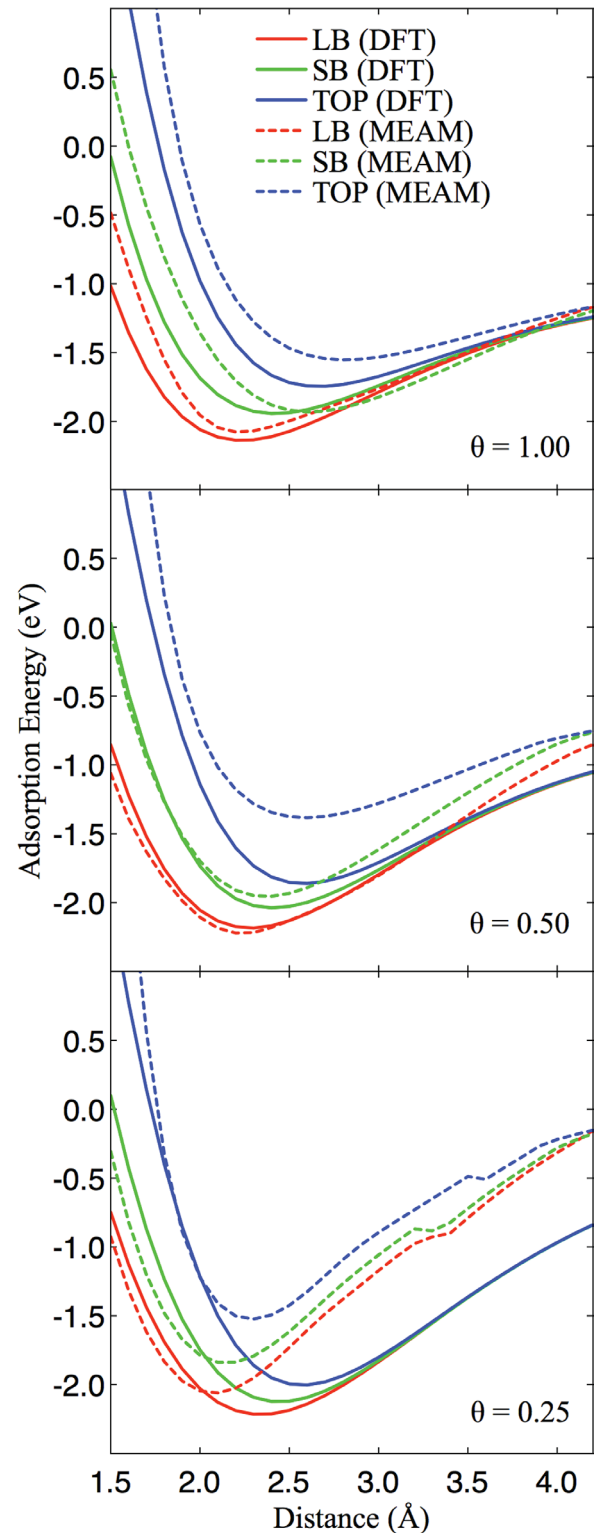
Figure 2. Adsorption energy curves of three adsorption sites of Li on the Mo (1 1 0) surface as a function of distance between the Li and Mo atoms for coverages, $\theta = 1.00$, $\theta = 0.50$, and $\theta = 0.25$. Solid lines are benchmark results from KSDFT calculations, while dashed lines represent the results obtained from the new 2NN MEAM Li–Mo force field.

distances are within 0.2 Å. The largest deviations between KSDFT and 2NN MEAM calculations occur for the TOP site. However, this site is not stable (it is a saddle point) and will

Table 2. Adsorption energies, E_{ads}, (in eV) and Li–Mo distances, h, (in Å) of different adsorption sites and coverages (θ) of Li on the Mo (1 1 0) surface from both KSDFT and 2NN MEAM calculations.

	DFT			MEAM		
θ	E_{ads}(LB)	E_{ads}(SB)	E_{ads}(TOP)	E_{ads}(LB)	E_{ads}(SB)	E_{ads}(TOP)
1.00	−2.149	−1.950	−1.794	−2.094	−1.952	−1.586
0.50	−2.222	−2.068	−1.930	−2.224	−1.956	−1.384
0.25	−2.254	−2.158	−2.069	−2.062	−1.844	−1.524
θ	h(LB)	h(SB)	h(TOP)	h(LB)	h(SB)	h(TOP)
1.00	2.229	2.413	2.663	2.211	2.523	2.731
0.50	2.250	2.377	2.482	2.239	2.367	2.592
0.25	2.308	2.397	2.482	2.076	2.147	2.288

be less important in classical MD simulations than the more stable sites.

As a second test, we ran both KSDFT and classical MD simulations for a system consisting of 32 Li atoms and 40 Mo atoms. The initial geometry was four layers of (2×2) Li on five layers of Mo placed on a bcc lattice oriented to expose the (1 1 0) surface to vacuum. Again, the vacuum region extended 10 Å in the z direction so the slab did not interact with its periodic images in this direction. The bottom three layers of Mo were held fixed. We chose a $8.92 \times 6.31 \times 40.00$ Å^3 cell with the [1 1 0] direction parallel to the z axis. Periodic boundary conditions were used in both MD simulations. A time step of 0.2 fs was used. The Nosé–Hoover thermostat [28, 29] was used in both MD simulations to keep the temperature at 470 K, which is slightly higher than the experimental ambient pressure bulk melting temperature of Li of 454 K [30]. We note that the Li 2NN MEAM force field by Cui *et al* [17] has been shown to have a bulk melting temperature of about 443 K [31] at ambient pressure, which is in reasonable agreement with experiment. The bulk melting temperature of Li is significantly lower than that of Mo. At ambient pressure, the experimental bulk melting temperature of Mo is 2896 K [32], while the bulk melting temperature for the Mo 2NN MEAM force field by Lee *et al* is estimated to be 3100 K [15]. Although the Mo force field seems to overestimate the melting temperature by approximately 7%, it accurately captures other physical properties such as crystal structure energy orderings and surface energies [15]. For both methods, a 24-ps trajectory was run. Configurations from the final 15 ps were used to compute the ionic density profiles. Larger systems sizes were not examined due to the computational cost of KSDFT MD. The ionic density profiles from the two MD simulations are shown in figure 3.

Results from both methods are in excellent agreement for both Mo and Li layers, highlighting the accuracy of the newly tuned Li–Mo MEAM force field. We note that the number of Mo layers remains the same over the course of the simulation, however the Li atoms rearrange themselves increasing from four layers to five. The peak associated with the first Li layer (adjacent to the Mo substrate) is much sharper than the other four peaks of Li layers, suggesting a more solid-like feature possessed by the first Li layer. This will be explored in more detail in later sections. The preceding results illustrate that the new Li–Mo force field accurately reproduces the properties used in the optimization procedure and is robust enough to capture structural properties of Li on the Mo (1 1 0) surface.
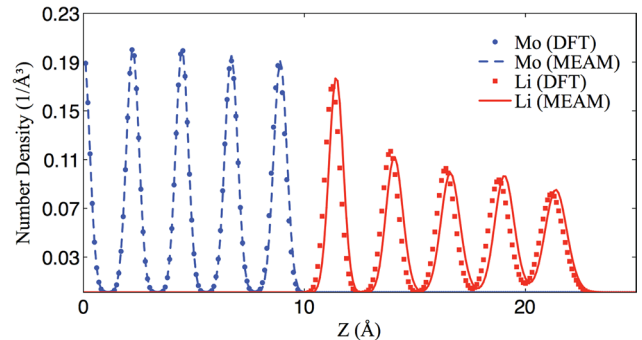
Figure 3. Ionic density profiles obtained from KSDFT and 2NN MEAM MD simulations at 470 K. The KSDFT and 2NN MEAM results for three leftmost Mo peaks match exactly because these layers are held fixed.

3. Classical simulations

3.1. Droplet simulation

In an attempt to study the contact angle of liquid Li on the Mo (1 1 0) surface, classical MD simulations of a Li droplet on Mo substrates were performed. A time step of 0.5 fs was used for all following simulations in this work. First, a slab of Mo atoms were arranged on a bcc lattice in a periodic box with the [1 1 0] direction oriented in the z direction. The slab was exposed to a vacuum region that extended approximately 175 Å in the z direction. This vacuum region was large enough such that the slab did not interact with its periodic images through this dimension. The slab contained 39 168 Mo atoms in twelve layers. The Mo slab was equilibrated by performing a MD simulation in the NVT ensemble. Temperature was maintained using the Nosé–Hoover thermostat [28, 29], and the lengths of the simulation box in the x and y directions were commensurate with the lattice spacing of Mo at the temperature being simulated. (The temperature dependence of the lattice spacing of bcc Mo was determined by performing separate bulk NPT simulations at zero pressure using the Nosé–Hoover thermostat [28, 29] to maintain temperature and the Nosé–Hoover barostat [33, 34] to maintain the pressure.) The atoms in the bottom six layers of the slab were fixed during the equilibration to simulate a semi-infinite crystal. An equilibration of 1000 ps was found to be sufficient for the Mo slab to reach equilibrium, as determined by the fact that the potential energy did not drift from a time-independent average for the remainder of the simulation time. This monitoring of
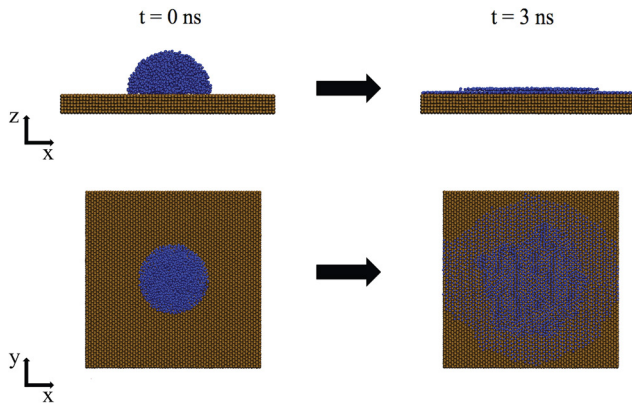
Figure 4. Snapshots from a simulation of a Li droplet on the Mo (1 1 0) surface at 460 K. Blue spheres are Li atoms and brown spheres are Mo atoms. The bottom six layers of Mo that are held fixed are not shown. Snapshots in the top row show a side view of the simulation, while the bottom row shows a top-down view of the same simulation. Snapshots in the left column are the initial condition, while snapshots in the right column are after 3 ns. Snapshots were rendered in VMD [26].

the potential energy was done for all classical simulations in this work to check that equilibrium was achieved.

A separate bulk simulation of liquid Li was run in the NVT ensemble, again using the Nosé–Hoover thermostat [28, 29] to maintain the temperature at a constant value. The volume of the box was chosen to match the average density of bulk liquid Li simulations run in the NPT ensemble (using the Nosé–Hoover thermostat [28, 29] and Nosé–Hoover barostat [33, 34]) at zero pressure and the specified temperature. The NVT simulation was found to reach equilibrium after 375 ps.

Using the final snapshot of the liquid Li simulation, a hemisphere was cut out containing about 2500 atoms and placed 2 Å above the Mo (1 1 0) surface from the aforementioned Mo slab simulation. A vacuum region that extended approximately 150 Å in the *z* direction was present above the top of the Li hemisphere. This region was large enough such that the slab and the droplet did not interact with their periodic images in the *z* direction because the cutoff distance for the force field is only 4.8 Å. This system was then allowed to run in the NVT ensemble using the Nosé–Hoover thermostat [28, 29] to keep the temperature constant. All of the aforementioned simulations were run at 460 K. This temperature was chosen because it is slightly above the bulk melting temperature of Li at ambient pressure and therefore represents a lower limit on the operating temperature for Li as a plasma-facing material. Initial and final configurations of the droplet simulation at 460 K are shown in figure 4.

The simulation shows that liquid Li perfectly wets the (1 1 0) surface of Mo at 460 K, when described by the force fields used in this work. The Li droplet has spread to cover most of the Mo surface after 3 ns. We expect similar behavior when the temperature is increased above 460 K, even though we did not perform droplet simulations at higher temperatures. This is because the experimental work by Fiflis *et al* [13] shows that, independent of both the solid substrate and its treatment, the contact angle of liquid Li tends to decrease

as temperature increases, indicating progressively better wetting behavior.

In the context of plasma-facing materials, this suggests liquid Li will perfectly wet the inside wall of a tokamak reactor if it is composed of Mo. Our simulation results contradict experimental results by Fiflis *et al* that show Li has a non-zero contact angle on Mo [13]. However, there are two important differences between the simulations and experiments. The first is that despite being performed in a vacuum environment to minimize the amount of oxygen present, there was still enough oxygen present in the experimental chamber for the oxidation rate to be significant at the temperatures examined. This has been found to have a significant effect on the wetting properties of Li on Mo [13]. The second is the fact that our droplet simulations were performed on a perfect Mo (1 1 0) surface, while the macroscopic experiments were performed on a polycrystalline Mo surface. The presence of grain boundaries and other exposed surfaces that do not correspond to the (1 1 0) surface could also have an effect on the wetting properties. The discrepancy between the experimental and simulation results presented in this paper warrant further investigation on how the presence of grain boundaries and surface defects affects the wetting of Li on Mo. It should be noted that there have been simulation studies on certain systems that have found that the contact angle depends on the size of the droplet being used [35]. This has not been explored in detail in this work due to the computational cost of these simulations. It is possible that the system size used in this work also contributes to the discrepancies between our simulations and the experimental results of Fiflis *et al* [13].

The snapshot in the top-right corner of figure 4 reveals that the Li atoms show some degree of ordering after they have spread on the Mo (1 1 0) surface. The degree of solid-like behavior of these atoms motivates studying the liquid Li-solid Mo (1 1 0) interface. However, instead of using droplet simulations to study this phenomenon, a thin-film geometry was used. Simulations with this new geometry are described in the next section.

3.2. Thin-film simulations

Similar to the construction of the initial configuration for the droplet simulations, for the thin-film simulations a slab of Mo atoms was first arranged on a bcc lattice with the [1 1 0] direction oriented in the *z* direction. The slab contained 21 000 Mo atoms in twelve layers. The bottom six layers in the slab were again held fixed in order to simulate a semi-infinite crystal. The simulation box was periodic in the *x* and *y* directions, and the lengths of the box in these directions were again set to be commensurate with the lattice spacing of Mo at the temperature being simulated. The Mo slab was covered with a thin film of 21 000 Li atoms. Above the Li atoms was a vacuum region that extended approximately 150 Å in the *z* direction. This vacuum region was again large enough such that the thin-film configuration did not interact with its periodic images in the *z* direction. Initially, these atoms were placed on a perfect bcc lattice on top of the Mo slab using the same lattice spacing of the Mo at the temperature of simulation. At all temperatures
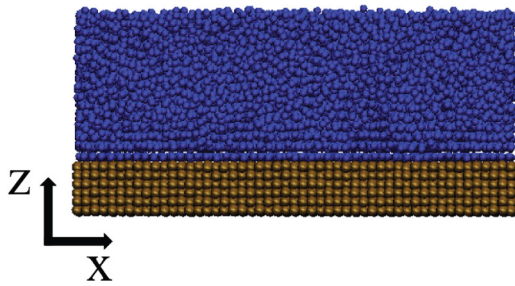
Figure 5. A snapshot from a simulation of a Li thin film on the Mo (1 1 0) surface at 460 K. Blue spheres are Li atoms and brown spheres are Mo atoms. The bottom six layers of Mo that are held fixed are not shown. The snapshot was rendered in VMD [26].

examined, the Li atoms quickly melted during the equilibration period. The system was equilibrated for 500 ps which was more than enough time for the energy to stabilize. A production period of 1500 ps followed equilibration to calculate properties of the Li thin film. A snapshot of an equilibrated thin-film simulation is shown in figure 5.

The thin-film simulations were conducted at three temperatures: 460, 700, and 1500 K in the NVT ensemble. The first temperature was chosen because this is slightly above the bulk melting temperature of lithium at ambient pressure (454 K) [30]. The second was chosen because it is close to an approximate operating temperature limit of a liquid lithium plasma-facing material [36]. The last temperature was chosen to test the limits of the solid-like behavior exhibited by the first Li layer on the Mo surface. In each case temperature was maintained using the Nosé–Hoover thermostat [28, 29]. Although it would be interesting to examine the behavior of the Li thin film at other temperatures, the computational cost of these simulations was too high for such studies to be undertaken as part of the present work. We believe, however, that our results present a reasonably comprehensive qualitative framework for the temperature-dependent behavior of the Li film.

For the simulation at 1500 K, it was found that Li atoms would eventually evaporate from the thin-film, making it difficult to study the properties of the film. This is expected since 1500 K is well above the temperature at which Li quickly evaporates under a vacuum. This is supported by the temperature-programmed desorption results by Chen *et al* [14]. A repulsive wall was placed at the top of the simulation box in order to keep atoms in the film. Atoms interacted with the repulsive wall through a truncated and shifted 9–3 Lennard-Jones potential with $\epsilon = 0.01$ eV, $\sigma = 1.0$ Å, and a cut-off distance of 2.5 Å.

During the thin-film simulations, 10 000 snapshots were stored during the production period. The density profile of Li was calculated from these snapshots. The results for 460, 700, and 1500 K are shown in figure 6.

Li exhibits strong density oscillations near the Mo slab, which was also seen in figure 3. The amplitude of the oscillations decreases as distance from the Mo slab is increased. Increasing temperature also decreases the amplitude of the oscillations. In all cases the films are thick enough to reach the bulk liquid density of Li at the corresponding temperature. At 460 and 700 K, the Li density profiles drop off to
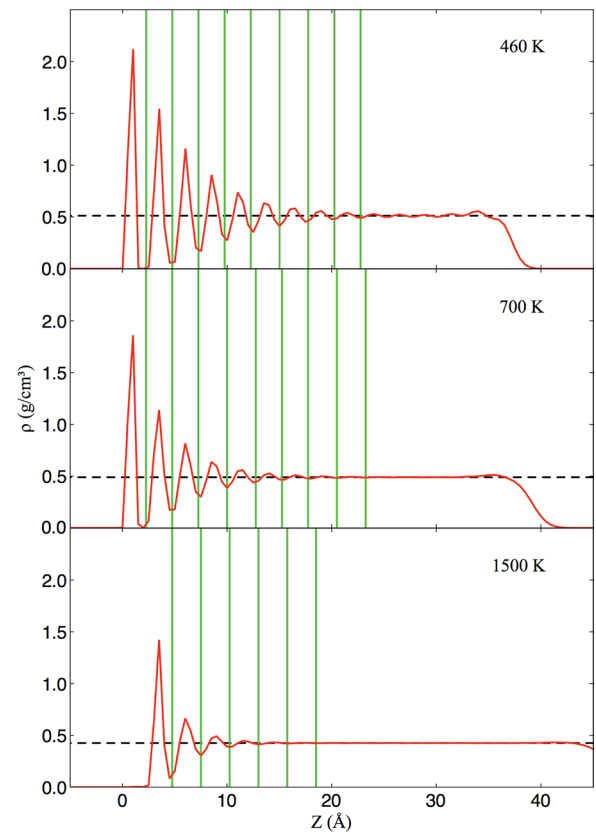

Figure 6. Density profiles of Li on the Mo (1 1 0) surface at various temperatures are shown as red solid lines. Li is in contact with Mo on the left-hand side of the plots; however, the density profiles for Mo are not shown. Black dotted lines correspond to the bulk density of liquid Li at the given temperature. Vertical green solid lines denote layer boundaries. These boundaries were placed at the minima of the Li density profiles.

zero beyond a thickness of ca. 35–40 Å. This is roughly the location of the Li-vacuum interface. For 1500 K, the Li film has expanded such that this interface is located beyond 45 Å and is therefore not seen in the figure. 'Layers' of liquid Li are defined based on the density oscillations. The boundaries of these layers are shown in figure 6 as solid green vertical lines. These boundaries are located at the minima of the Li density profiles. A variety of analyses were performed for Li atoms in these layers in order to investigate whether they exhibited solid-like or liquid-like behavior. The type of analyses and results will be explained below.

The two-dimensional radial distribution function (2D RDF) ($g^{2D}(L, R)$) for a given layer L can been calculated for each of layers by the equation used by Broughton and Woodcock [37]. The mathematical form of $g^{2D}(L, R)$ is given in the appendix. Results are shown in figure 7.

At 460 K, the 2D RDF for layer 1 shows a degree of long-range ordering as indicated by the presence of peaks at long distances. This suggests that the structure of layer 1 contains solid-like characteristics. The 2D RDF of layer 2 exhibits a widening and shifting of peaks relative to the 2D RDF in layer 1, therefore there is less long-range order present in this layer. The 2D RDFs of layers 3 through 6 are very similar and only display peaks at short distances, indicating a liquid-like
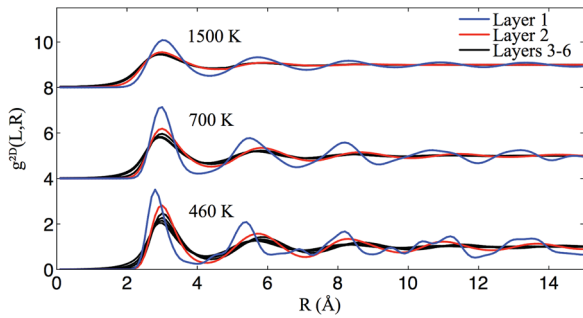
Figure 7. Two-dimensional radial distribution functions of different layers of Li on the Mo (1 1 0) surface at various temperatures. The functions for 700 and 1500 K have been vertically shifted for clarity. Layer 1 corresponds to the layer of Li closest to the Mo substrate, while layer 6 is the layer furthest away of those analyzed.

structure in these layers. At 700 K, the 2D RDF for layer 1 exhibits smaller peaks when compared to the same layer at 460 K; however, the peaks are still present at long distances suggesting the layer is still solid-like at this temperature. The 2D RDFs of layers 2 through 6 indicate a liquid-like structure. At 1500 K, the 2D RDF for layer 1 is more representative of liquid structure. However, it still differs significantly from the 2D RDFs for layers 2-6 at this temperature, showing that there is still some ordering in layer 1 imposed by the Mo surface.

The intra-layer mobility of Li atoms was examined by measuring the mean-squared displacements (MSDs) in directions parallel to planes that define the layers. This includes the *x* and *y* directions of figure 5 (where the *y* direction points into the page). The calculation of the lateral MSDs for a given layer requires the definition of an ad hoc MSD, $\Psi_k(L,t)$, due to the fact that atoms are free to move between layers. In this work, $\Psi_k(L,t)$ is defined as the lateral MSD of particles that are present in layer *L* at the start of the production period ($t = 0$) and at time, *t* [38]. The subscript *k* is either *x* or *y*, corresponding to movement in these directions respectively. The mathematical definition of the ad hoc MSD used in this work can be found in the appendix. This definition is computationally convenient for examining anisotropies in mobility and has been applied to other systems such as the Kob–Andersen binary Lennard-Jones in a thin-film [39].

Results for the MSD in the *x* direction are shown in figure 8. Results for the *y* direction are similar and are therefore not shown here.

At all temperatures, the MSDs of the Li atoms in layers 3 through 6 show liquid-like behavior. That is, there is a ballistic regime at short times and a diffusive regime at longer times. At 460 K, layer 2 exhibits lower lateral mobility than layers 3 through 6 for a majority of the simulation time due to its proximity to the Mo surface. The Li atoms in layer 1 have an MSD orders of magnitude below other layers for the entire simulation time. At 700 K, the MSD for layer 2 is essentially identical to the liquid-like MSDs for layers 3 through 6. Layer 1 still has an MSD orders of magnitude lower than the other layers, however the atoms in this layer are noticeably more mobile than at 460 K. At 1500 K, the Li atoms in layer 1 still do not show a typical liquid MSD; however, the atoms are significantly more mobile.
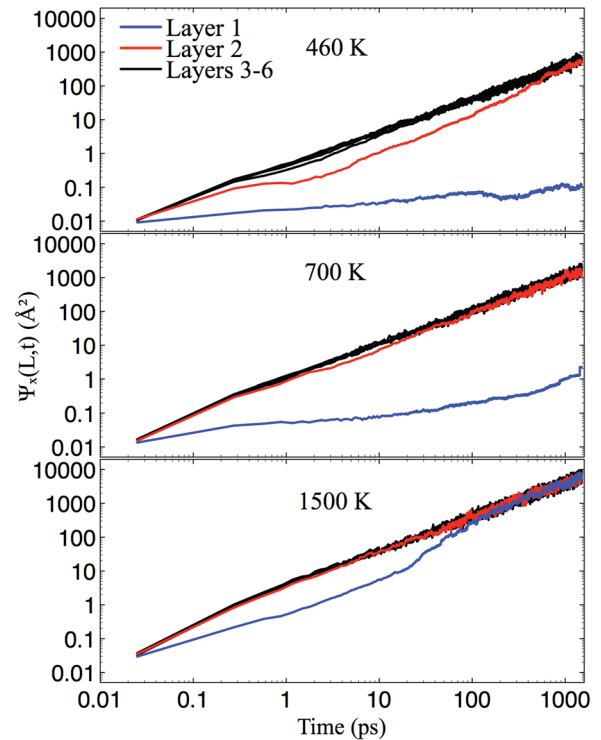
Figure 8. *Ad hoc* mean-squared displacement of different layers of Li on the Mo (1 1 0) surface at various temperatures. Only the mean-squared displacements along the *x* direction of the simulation cell are shown.

Table 3 gives the times at which the ad hoc MSDs are equal to 1.0 Å^2 for layers 1 through 6 at various temperatures. Results are given for both the *x* and *y* directions. We note that for a given layer number and temperature, the times required for the MSD to reach 1.0 Å^2 are similar for both the *x* and *y* direction. We also note that there are no times reported for the MSDs for layer 1 at 460 K because they did not reach 1.0 Å^2 over the timescale of the simulation.

The ability of Li atoms to migrate between layers was studied by examining the evolution of the quantity we denote as $M(L,t)$ as a function of time. $M(L,t)$ is the number of atoms present in layer *L* both at the beginning of the measurement window and at time *t*. We note that it was not practical to simply study $\Psi_z(L,t)$ because the width of the layers were thin enough that, for most layers, atoms leave their original layers quickly. This was especially true for layers far from the Mo slab and at high temperatures. Therefore, $\Psi_z(L,t)$ is only able to be measured with high precision at short times.

The results for the first layer are shown in figure 9.

At 460 K, essentially none of the Li atoms originally present in layer 1 leave the layer over the course of the simulation. At 700 K, Li atoms are shown to migrate to other layers, but in a much less dramatic fashion when compared to 1500 K. At 1500 K, $M(L,t)$ quickly decays before saturating to an equilibrium value. We can define the 'lifetime' of the layer as the time when the layer has lost 90% of the atoms originally present. This is shown as the vertical red dotted line in figure 9.

The results for the second layer are shown in figure 10.

Table 3. Time (ps) at which the ad hoc mean-squared displacements of different layers of Li is equal to 1.0 $\overset{\circ}{A}^2$ on the Mo (1 1 0) surface at various temperatures.

|	$\Psi_x(L,t)$			$\Psi_y(L,t)$		
	460 K	700 K	1500 K	460 K	700 K	1500 K
Layer 1	—	832.13	2.03	—	703.90	2.00
Layer 2	9.05	1.15	0.35	9.85	1.13	0.33
Layer 3	3.28	0.80	0.33	3.85	0.93	0.30
Layer 4	2.65	0.80	0.30	2.40	0.95	0.30
Layer 5	2.33	0.93	0.28	2.33	0.93	0.30
Layer 6	2.10	1.03	0.35	1.90	0.95	0.30
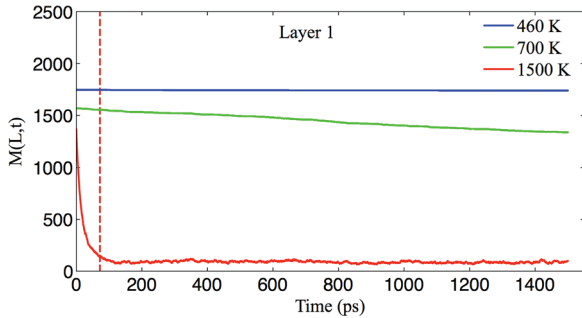
Figure 9. Number of atoms that remain in the 1st layer of Li on the Mo (1 1 0) surface as a function of time at various temperatures. The vertical dotted line indicates the time at which 90% of the atoms originally present have left the layer at 1500 K.

In contrast to layer 1, layer 2 sees a rapid migration of Li atoms at all temperatures, not just at 1500 K. At all three temperatures, $M(L,t)$ shows the same qualitative behavior. The layer lifetimes for layer 2 at each temperature can be calculated and are shown in figure 10 as the vertical dotted lines. It is not surprising to see that the layer lifetime decreases when temperature is increased.

The same lifetime analysis can be performed on other layers in the Li thin film. The lifetimes for layers 1 through 6 are given in figure 11 as a function of temperature on an Arrhenius plot. For layer 1, only one lifetime is given due to the fact that for this layer, $M(L,t)$ only decayed by 90% at 1500 K over the timescale of the simulation.

As stated earlier, the lifetime of a given layer decreases with increasing temperature. At a given temperature, the lifetime is shorter for layers further away from the Mo surface. This is to be expected as the Mo surface imposes a degree of solid-like behavior on the Li atoms closest to it.

The results of the analyses presented for the thin-film simulations indicate that the first layer of Li possesses many solid-like characteristics even at temperatures well above the bulk melting temperature. This is shown by the solid-like 2D RDFs, low interlayer mobilities, and longer layer lifetimes at 460 K and 700 K. Layer 2 exhibits behavior between a solid and liquid at 460 K, but is completely liquid-like at 700 K and 1500 K. Higher layers exhibit characteristics and behaviors of a liquid at all temperatures examined. This is reflected in the liquid-like 2D RDFs and high mobility of atoms in these layers.
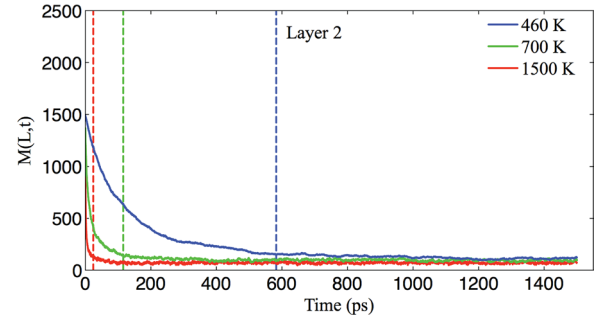
Figure 10. Number of atoms that remain in the 2nd layer of Li on the Mo (1 1 0) surface as a function of time at various temperatures. The vertical dotted lines indicate the time at which 90% of the atoms originally present have left the layer for each temperature.
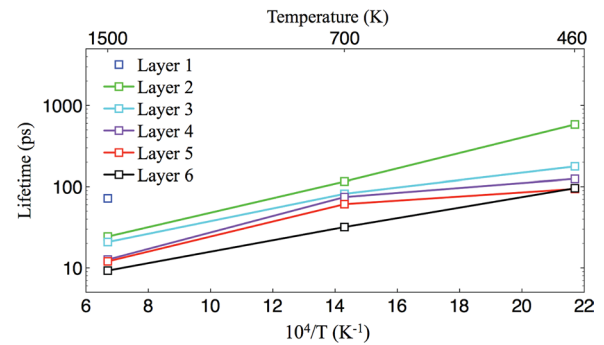
Figure 11. Lifetime of different layers of Li as a function of temperature. Connecting lines are guides to the eye.

4. Concluding remarks

In this work, a classical 2NN MEAM force field was developed for Li–Mo interactions by fitting to KSDFT calculations. The fitting procedure utilized adsorption energies and forces on Li atoms adsorbed on the Mo (1 1 0) surface at various coverages and adsorption sites to generate parameters for the 2NN MEAM potential. We performed two tests to validate the predictive power of the new force field. The first test involved calculating the adsorption energies and minimum energy distances at various adsorption sites and surface coverages. The new force field correctly reproduced the energy orderings between LB, SB, and TOP sites. The adsorption energies quantitatively agree for the LB site at high coverages, which is vital for studying the wetting properties of Li on the Mo (1 1 0) surface. There are deviations between the adsorption energies and Li–Mo distances between the new force field and KSDFT calculations with respect to Li occupying the TOP site. However, this is acceptable since the TOP site is not a stable adsorption site. In the second test, we performed KSDFT and classical MD simulations for a system containing 40 Mo atoms and 32 Li atoms at 470 K. The initial geometry was composed of five layers of Mo and four layers of Li. We found excellent agreement between the ionic density profiles generated from the two methods. These two examples demonstrate the ability of the new 2NN MEAM force field to describe the interface between liquid Li and the Mo (1 1 0) surface.

Using the new 2NN MEAM force field, a droplet simulation showed that liquid Li perfectly wets the Mo (1 1 0) surface at 460 K. This contradicts experimental results that have shown that Li has a non-zero contact angle on a Mo substrate. A possible explanation for this contradiction between our simulations and experiments is that the surface structure of Mo and the presence of oxygen and impurities have a significant effect on the contact angle.

Thin-film simulations were used to characterize the behavior of Li atoms in contact with the Mo (1 1 0) surface at 460, 700, and 1500 K. The density profile of liquid Li shows that there are strong density oscillations near the Mo (1 1 0) surface at all temperatures simulated. Layers of Li were defined based on these density oscillations. Several metrics were used to characterize the Li atoms in each of these layers. These metrics included 2D RDFs, intra-layer mobilities, and layer lifetimes, and allowed us to understand to what extent Li atoms exhibit solid-like or liquid-like behavior.

At 460 and 700 K, the 2D RDFs of the first layer of liquid Li in contact with the Mo surface shows a degree of ordering suggesting that this layer is solid-like at these temperatures, despite being above the bulk melting temperature of lithium at ambient pressure. This solid-like behavior is supported by the fact that the lateral mobility of the first layer is orders of magnitude below that of the other layers at 460 and 700 K. Examining layer lifetimes shows that the Li atoms in the first layer at the same temperatures do not migrate between layers as readily as the Li atoms in other layers, also supporting the solid-like behavior of the first layer at these temperatures. Only at higher temperatures (1500 K) does the first layer begin to exhibit liquid behavior. This demonstrates the strength of the adhesion of the first layer of Li on the Mo (1 1 0) surface. This strong adhesion is supported by temperature-programmed desorption experiments [14]. Other layers exhibit more liquid-like behavior, with the second layer showing characteristics intermediate between a solid and a liquid at 460 K.

The results in this work suggest that liquid Li is an excellent liquid metal plasma-facing material for tokamak fusion reactors if the inside walls are primarily composed of Mo. This is due to the fact that Li wets and strongly adheres to the Mo (1 1 0) surface. There are several possible future directions for MD studies related to the systems of interest. For example, one could investigate the wetting properties of other candidate liquid metal plasma-facing materials on Mo, such as tin, gallium, and lithium-tin alloys, and also how these wetting properties are affected by surface defects. Studies could also be performed on the wetting properties of other relevant solid substrates such as tungsten. Introduction of oxygen and hydrogen to the Li–Mo system would be interesting for two reasons. The first is that introduction of oxygen would possibly provide insight into the discrepancies between our simulations and the experimental results of Fiflis *et al* [13]. Second, consideration of oxygen and hydrogen are important because the presence of lithium hydroxide is an important concern in fusion devices. However, the introduction of these two elements presents a challenge because chemical reactions need to be considered. The 2NN MEAM formalism used in this work does not handle chemical reactions, therefore an improved formalism needs to be employed. Recently, the MEAM formalism has been improved to incorporate charge transfer and ionic bonding [40], and the Streitz–Mintmire potential has been used for metal oxides [41]. These force fields would be able to aid in these studies. Consideration of charge transfer may also improve the present Mo–Li force field. KSDFT calculations indicate a degree of charge transfer between Li and Mo when Li is adsorbed on the Mo (1 1 0) surface [14].

Careful force field development and validation is required for these studies. If developed properly, they would allow for comparisons between different combinations of liquid plasma-facing materials and solid substrates from a computational perspective. First-principles quantum mechanics calculations can guide parameter determination for classical potentials, as was the case for the present study.

Acknowledgments

Appendix A. 2D Radial distribution functions

As mentioned in the 'Thin-film simulations' section, the two-dimensional radial distribution function (2D RDF) ($g^{2D}(L, R)$) for a given layer L is calculated using the equation given by Broughton and Woodcock [37]. 2D RDFs were calculated using the same snapshots used for the density profiles.

$$g^{2D}(L, R) = \left\langle \frac{A}{N_L} \left[\frac{n(R, L)}{2\pi R \mathrm{d}R} \right] \right\rangle. \tag{A.1}$$

In this equation, A is the cross-sectional area of a layer, N_L is the number of Li atoms in layer L, and $n(R, L)$ is the number of atoms in layer L between R and $R + \mathrm{d}R$. R is the radial direction perpendicular to the z direction. Angular brackets denote an ensemble average.

Appendix B. Intra-layer mobilities

The mathematical definition of the ad hoc MSD, $\Psi_k(L, t)$, is given below.

$$\Psi_k(L, t) = \frac{1}{M(L, t)} \sum_{i=1}^{N} |r_i^k(t) - r_i^k(0)|^2 \mathcal{D}(z_i(0), z_i(t), L), \tag{B.1}$$

where $\mathcal{D}(z_i(0), z_i(t), L)$ is 1 if particle i is in layer L at the beginning of the production period and at time t, and 0 otherwise. $r_i^k(t)$ is the k component of the position vector for particle i at time t. $z_i(t)$ is the z position of particle i at time t.

$M(L, t)$ is the number of atoms present in layer L both at the beginning of the measurement window and at time t.

ORCID iDs

Joseph R. Vella ⓘ https://orcid.org/0000-0002-8666-8719
Mohan Chen ⓘ https://orcid.org/0000-0002-8071-5633
Emily A. Carter ⓘ https://orcid.org/0000-0001-7330-7554
Athanassios Z. Panagiotopoulos ⓘ https://orcid.org/0000-0002-8152-6615

References

[1] Lipschultz B., Pappas D.A., LaBombard B., Rice J.E., Smith D. and Wukitch S.J. 2001 *Nucl. Fusion* **41** 585
[2] Brooks J.N., Allain J.P., Whyte D.G., Ochoukov R. and Lipschultz B. 2011 *J. Nucl. Mater.* **415** S112
[3] Wong C.P.C., Chin E., Petrie T.W., Reis E.E., Tillack M., Wang X., Sviatoslavsky I., Malang S. and Sze D.K. 1997 *Fusion Eng. Des.* **38** 115
[4] Dux R. *et al* 2009 *J. Nucl. Mater.* **390–1** 858
[5] Lipschultz B., Coenen J.W., Barnard H.S., Howard N.T., Reinke M.L., Whyte D.G. and Wright G.M. 2012 *Nucl. Fusion* **52** 123002
[6] Coenen J.W., De Temmerman G., Federici G., Philipps V., Sergienko G., Strohmayer G., Terra A., Unterberg B., Wegener T. and Vanden Bekerom D.C.M. 2014 *Phys. Scr.* **2014** 014037
[7] Wells W.M. 1981 *Fusion Sci. Technol.* **1** 120
[8] Johnson D.F. and Carter E.A. 2010 *J. Mater. Res.* **25** 315
[9] Nygren R.E., Cowgill D.F., Ulrickson M.A., Nelson B.E., Fogarty P.J., Rognlien T.D., Rensink M.E., Hassanein A., Smolentsev S.S. and Kotschenreuther M. 2004 *Fusion Eng. Des.* **72** 223
[10] Hassanein A., Allain J.P., Insepov Z. and Konkashbaev I. 2005 *Fusion Sci. Technol.* **47** 686
[11] Brooks J.N., Rognilien T.D., Ruzic D.N. and Allain J.P. 2001 *J. Nucl. Mater.* **290–3** 185–90
[12] Allain J.P., Ruzic D.N. and Hendricks M.R. 2001 *J. Nucl. Mater.* **290–3** 33
[13] Fiflis P., Press A., Xu W., Andruczyk D., Curreli D. and Ruzic D.N. 2014 *Fusion Eng. Des.* **89** 2827
[14] Chen M., Roszell J., Scoullos E.V., Riplinger C., Koel B.E. and Carter E.A. 2016 *J. Phys. Chem.* B **120** 6110
[15] Lee B and Baskes M.I. 2000 *Phys. Rev.* B **62** 8564
[16] Plimpton S. 1995 *J. Comput. Phys.* **117** 1
[17] Cui Z., Gao F., Cui Z. and Qu J. 2012 *Modelling Simul. Mater. Sci. Eng.* **20** 015014
[18] Lee B., Baskes M.I., Kim H. and Cho Y.K. 2001 *Phys. Rev.* B **64** 181402
[19] Kresse G. and Hafner J. 1993 *Phys. Rev.* B **48** 13115
[20] Kresse G. and Furthmüller J. 1996 *Comput. Mater. Sci.* **6** 15
[21] Kresse G. and Furthmüller J. 1996 *Phys. Rev.* B **54** 11169
[22] Perdew J.P., Burke K. and Ernzerhof M. 1996 *Phys. Rev. Lett.* **77** 3865
[23] Blöchl P.E. 1994 *Phys. Rev.* B **50** 17953
[24] Monkhorst H.J. and Pack J.D 1976 *Phys. Rev.* B **13** 5188
[25] Methfessel M. and Paxton A.T. 1989 *Phys. Rev.* B **40** 3616
[26] Humphrey W., Dalke A. and Schulten K. 1996 *J. Mol. Graph.* **14** 33
[27] Kirkpatrick S., Gelatt C.D.Jr. and Vecchi M.P. 1983 *Science* **220** 671
[28] Nosé S. 1984 *J. Chem. Phys.* **81** 511
[29] Hoover W.G. 1985 *Phys. Rev.* A **31** 1695
[30] Boehler R. 1983 *Phys. Rev.* B **27** 6754
[31] Vella J.R., Stillinger F.H., Panagiotopoulos A.Z. and Debenedetti P.G. 2015 *J. Phys. Chem.* B **119** 8960
[32] Dinsdale A.T. 1991 *CALPHAD, Comput. Coupling Phase Diagr. Thermochem.* **15** 317
[33] Hoover W.G. 1986 *Phys. Rev.* A **34** 2499
[34] Melchionna S., Ciccotti G. and Holian B.L. 1993 *Mol. Phys.* **78** 533
[35] Burt R., Birkett G., Salanne M. and Zhao X.S. 2016 *J. Phys. Chem.* C **120** 15244
[36] Majeski R 2010 *AIP Conf. Proc.* **1237** 122
[37] Broughton J.Q. and Woodcock L.V. 1978 *J. Phys. C: Solid State Phys.* **11** 2743
[38] Lançon P., Batrouni G., Lobry L. and Ostrowsky N. 2002 *Physica* A **304** 65
[39] Haji-Akbari A. and Debenedetti P.G. 2014 *J. Chem. Phys.* **141** 024506
[40] Lee E., Lee K., Baskes M.I. and Lee B. 2016 *Phys. Rev.* B **93** 144110
[41] Streitz F.H. and Mintmire J.W. 1996 *Phys. Rev.* B **50** 11996